Chemically ordered MnPt ultrathin films on Pt(001) substrate: Growth, atomic structure, and magnetic properties

Márcio M. Soares,* Maurizio De Santis, Hélio C. N. Tolentino,† Aline Y. Ramos, Mohammad El Jawad, and Yves Gauthier
Institut Néel, CNRS et Université Joseph Fourier, BP 166, F-38042 Grenoble Cedex 9, France

Fikret Yildiz‡ and Marek Przybylski
Max-Planck-Institut für Mikrostrukturphysik, 06120 Halle, Germany

(Received 3 February 2012; revised manuscript received 13 April 2012; published 10 May 2012)

Ultrathin MnPt films have been grown on Pt(001) single crystals by alternate deposition of Mn and Pt and studied *in situ* by grazing incidence x-ray diffraction. The growth mode and chemical order strongly depend on the deposition conditions. At room temperature, a 3D growth mode for Pt leads to a disordered and rough MnPt film. After annealing at 770 K, chemical order develops with the tetragonal axis oriented in the surface plane. At 570 K, Pt grows in a quasi layer-by-layer mode. For all depositions, and even after annealing, Mn remains essentially at the surface with negligible diffusion into bulk. As a consequence, the film deposited at 570 K is chemically ordered, with the tetragonal axis oriented mainly perpendicular to the surface. Coupled to ferromagnetic layers with in-plane (out-of-plane) anisotropy, these ultrathin (≈3 nm) MnPt films exhibit exchange bias properties and enhanced coercivity at low temperature.

DOI: 10.1103/PhysRevB.85.205417 PACS number(s): 68.55.−a, 75.50.Ss, 75.70.−i, 61.05.cp

I. INTRODUCTION

Antiferromagnetic (AFM) materials have been extensively investigated for their pinning effect when exchange-coupled with ferromagnetic (FM) ones. The coupling at the AFM/FM interface leads to an increase of the FM coercive field and, eventually, to a unidirectional anisotropy, the exchange bias (EB) effect.[1] The robustness of the exchange coupling depends on intrinsic parameters of the AFM material, such as spin configuration, anisotropy strength, exchange stiffness and Néel temperature but also on the quality of the interface.[2–4] While in the disordered cubic (fcc) phase MnPt alloy does not show special interest for technological applications, the tetragonal (fct) MnPt alloy in the chemically ordered $L1_0$ phase is one of the best AFM materials at room temperature (RT). Due to its high ordering temperature ($T_N = 975$ K)[5] and anisotropy strength, it is already largely used as the pinning layer in spin valves and tunnel junctions.[6]

The $L1_0$ phase consists of monoatomic layers (ML) of Mn and Pt alternating along the tetragonal c axis (see Fig. 1). Within the Mn (001) planes, nearest neighbors are antiferromagnetically coupled, while along the c axis they are ferromagnetically coupled. Mn spins are parallel to the c axis at RT.[5] Such uniaxial anisotropy is promising for perpendicular exchange coupled devices, provided that $L1_0$ MnPt films with out-of-plane (OP) c-axis orientation can be produced and coupled to FM ones also with perpendicular magnetic anisotropy (PMA).[7–9] The spectacular magnetic properties of the MnPt films are then directly related to their chemical order. In magnetic devices, the conservation of functional properties in films of still reduced thickness is of utmost importance. At the present time, the difficulty in producing well ordered ultrathin films (<10 nm) is one of the major limiting factors in the development of exchange bias devices.[10–12] In order to optimize exchanged coupled bilayers, in particular, with OP anisotropy, the understanding of the growth process of ultrathin MnPt films is a major issue to address.

The Pt(001) surface is well suited for the coherent epitaxial growth of MnPt films. The Pt lattice parameter ($a_{Pt} = 3.924$ Å) lies between the bulk $L1_0$ MnPt cell parameters, $a_{MnPt} = 4.002$ Å (2.0% > a_{Pt}), $c_{MnPt} = 3.665$ Å (6.6% < a_{Pt}).[13] The smaller mismatch with a_{MnPt} favors the OP c-axis orientation. Moreover, for pseudomorphic epitaxial films ($a_{MnPt} = a_{Pt}$) at constant volume, the $(c/a)_{MnPt}$ ratio should increase from 0.92 (bulk value) to 0.97. This constraint is expected to further increase the MnPt uniaxial anisotropy.[14] A drawback of the clean Pt(001) surface is its topmost layer quasihexagonal reconstruction. This reconstruction, usually referred as Pt(001)-hex, is incommensurate with the substrate and forms rows with angles of about 0.75° with the underling square rows. The hexagonal layer is 25% denser than the {001} cubic planes and nearly 8% denser than the {111} bulk close-packed planes.[15] When adatoms (e.g., CO and O_2,[16] Co,[17] Fe,[18] or Mn[19]) are chemisorbed, the reconstruction is lifted and the surface changes back to a Pt(001)-(1 × 1) bulklike structure. During this phase transformation, called deconstruction, the excess Pt atoms are forced up to mix with the adatoms. Deconstruction should then play an important role in the growth process of the earliest adlayers.

In this paper, we present an *in situ* grazing incidence x-ray diffraction (GIXRD) study of the mechanism of Mn, Pt, and MnPt growth on Pt(001) single crystal, with varied deposition conditions. First of all (Sec. II), we report the experimental conditions and the methodology. In the second part (Sec. III), we present the earliest stages of Mn and Pt growth and evaluate the consequences of the Pt(001)-hex reconstruction on the growth of the adlayers. The growth of MnPt films by alternate deposition at different temperatures are presented in Sec. IV and their magnetic properties, when coupled to FM layers, in Sec. V. The main results are finally discussed and summarized in Sec. VI.

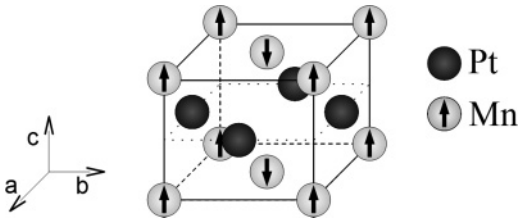

FIG. 1. Sketch of the chemically ordered $L1_0$ MnPt alloy. The AFM structure with Mn spins aligned along the c axis yields Mn planes of compensated spins.

II. EXPERIMENTAL

In situ GIXRD experiments were carried out at the UHV station of the French CRG BM32 beamline at the European Synchrotron Radiation Facility (ESRF). The station consists of a UHV chamber with base pressure 5×10^{-11} mbar mounted on a z-axis diffractometer with extra degrees of freedom for sample alignment. The chamber is equipped with standard tools for surface preparation, film deposition and characterization.[20] Prior to metal deposition, the Pt(001) surface is cleaned by several cycles of Ar^+ ion sputtering and annealed at 1170 K for 10 min, followed by a 5 min annealing at 970 K under 2×10^{-7} mbar of oxygen. Finally, the surface is flash annealed at 1170 K and slowly cooled down. The cleanliness of the surface is checked by Auger spectrometry and by GIXRD from the development of the Pt(001)-hex reconstruction.

High-purity Mn and Pt were deposited from an effusion cell, with an alumina crucible heated at about 1000 K, and from a water-cooled electron beam evaporator, respectively. The pressure rises to 5×10^{-10} mbar while operating the sources. The evaporation rate is calibrated with a quartz crystal microbalance and cross checked during a calibration deposition by measuring the oscillation period of the x-ray scattering intensity at the antiphase reciprocal space point of a crystal truncation rod (CTR).[21,22] The deposition rates were 0.18 ML/min for Mn and 0.04 ML/min for Pt. The estimated error bar in these rates is smaller than 10%.

X-ray diffraction reflections were collected using 20 keV monochromated photons under a grazing incidence of 0.6°, about three times the critical angle for total reflection. The x-ray reflections are indexed using a tetragonal surface unit cell with $a_S = b_S = (1/\sqrt{2})a_{\mathrm{Pt}}$ and $c_S = a_{\mathrm{Pt}}$. The surface reflection indexes (capital letters) are related to the fcc ones by $H = \frac{1}{2}(h - k)$, $K = \frac{1}{2}(h + k)$, $L = l$. The intensity for each $(H\ K)$-CTR is obtained either by integrating the distribution measured by angular scans of the sample about its surface normal, i.e., by rocking scans at each $(H\ K\ L)$ reciprocal space point,[21,23] or by performing fast continuous L scans along the crest of the $(H\ K)$-CTR.[24]

During the experiments, several equivalent rods are measured. They are then symmetry averaged. Structure factor amplitudes are extracted by applying standard corrections and error bars are estimated from their agreement factor.[23,25] Extraction of the structure factor amplitudes and surface structure fitting are performed using the ANA-ROD package.[26] The size of terraces, Pt(001)-hex domains and chemically ordered domains are obtained from the full width at half maximum (FWHM) of diffraction peaks for rocking and L scans using the Scherrer equation.[27]

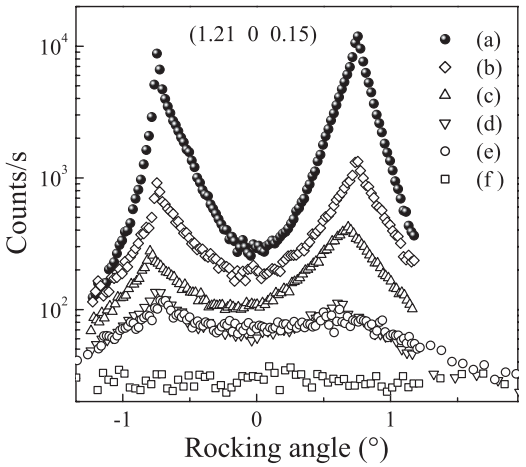

FIG. 2. Rocking scans around the (1.21 0 0.15) reciprocal space point of the Pt(001)-hex reconstruction rod for selected surfaces: (a) freshly clean surface; (b) immediately after 0.35-ML Mn deposition (19%); (c) 0.35-ML Mn after 10 hours (8%); (d) 0.35-ML Mn after 30 min annealing at 520 K (3%); (e) 1.2-ML Mn deposition on a freshly clean surface (2%); and (f) 1.2-ML Mn + 1-ML Pt (0%). The number in parenthesis is the remaining percentage of Pt(001)-hex reconstruction relative to the freshly clean surface.

III. EARLIEST STAGES OF Mn AND Pt GROWTH

After the cleaning procedure the crystal surface is rather flat, with terraces of about 900 nm, and covered by Pt(001)-hex domains with typical correlation length of 150 ± 50 nm. Figure 2(a) shows a rocking scan of the clean reconstructed surface about the (1.21 0 0.15) reciprocal space point. The two peaks correspond to two symmetric domains rotated by an angle $\theta = 0.74°$ from the [1 0] direction. The same rocking scans were collected at different stages of the Mn deposition. Taking the integrated intensity of each scan as a measure of the reconstructed surface and normalizing it to the fully reconstructed clean surface, we obtain at each stage an estimate of the remaining reconstruction (see Fig. 2).

A. 0.35 ML Mn deposited at RT

Immediately after 0.35-ML Mn deposition, the reconstruction is reduced to 20% compared to the clean surface [see Fig. 2(b)], dropping to about 10% after 4 hours. The deconstruction then proceeds at a slower rate. After 10 hours, the surface keeps nearly 8% reconstructed [see Fig. 2(c)]. The reduction of the reconstruction goes along with a stabilization of the Pt(001)-(1×1) surface. At the same time, faint $c(2 \times 2)$ superlattice peaks show up at half-integer reflection indexes. We have also observed these peaks by LEED for samples grown in similar conditions (see Fig. 3.5 in Ref. 28). These features suggest that Mn adatoms mix with Pt atoms to form an ordered chessboard-like MnPt-$c(2 \times 2)$ surface alloy, as observed for submonolayer Mn deposition on several metallic substrates.[29]

In order to obtain a quantitative description of the layer formed on the Pt(001)-(1×1) surface, we analyzed a complete

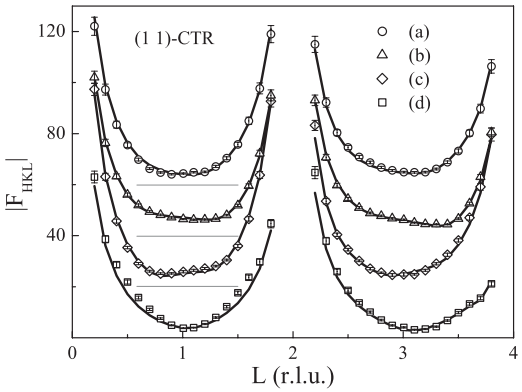

FIG. 3. Experimental (symbols) and fitted (solid black lines) structure factor amplitudes of the (1 1)-CTR for the (a) 0.35-ML Mn film deposited at RT, (b) idem after annealing at 520 K, (c) 1.2-ML Mn film deposited at RT and (d) 1-ML Pt deposited on the previous film at RT. The rods are shifted vertically by 20 units for clarity. Gray lines indicate the zero for shifted rods.

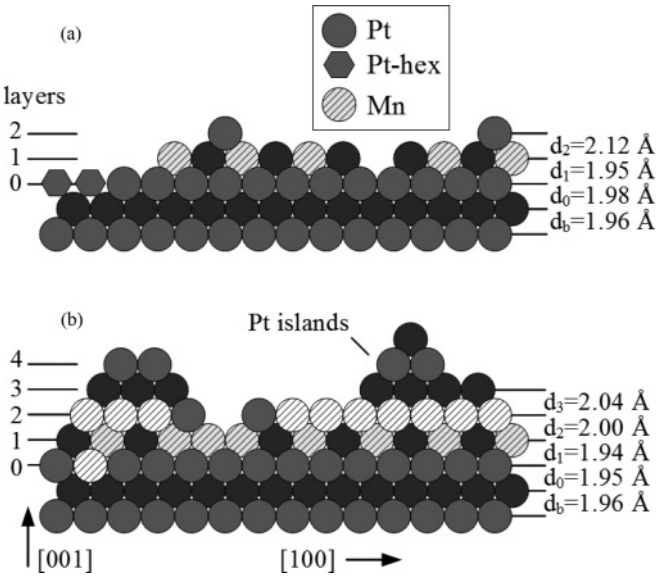

FIG. 4. Sketch of the model structure for the (a) 0.35-ML Mn and (b) 1-ML Pt/1.2-ML Mn, deposited at RT on Pt(001)-hex. The distances obtained by fit are given. The sketch (a) shows some remaining reconstruction, but no Mn atoms, in layer 0, and a MnPt-$c(2 \times 2)$ surface alloy in an incomplete layer 1. (b) shows the same ordered alloy with the layer 1 completed by Mn atoms, the excess of Mn covering partially the layer 2 and the 3D growth of islands after Pt deposition.

set of data along integer $(H\ K)$-CTRs collected in the interval of 4 to 10 hours after deposition. In the model used in the fitting procedure, the layers are numbered with increasing indexes from substrate to the surface. We give the index 0 to the initially reconstructed overlayer, Pt(001)-hex, that transforms into Pt(001)-(1×1). This layer may contain some deposited Mn atoms. The other adlayers are labeled with successive indexes. The main fitting parameters are the distances d_n (distances between layer n and the precedent one) and the atomic occupancies of Mn (θ^n_{Mn}) and Pt (θ^n_{Pt}) in each layer. A Debye parameter (B) takes into account the thermal and structural disorders. Distinct B parameters are fitted for each layer, while for the substrate, the B parameter is set to the bulk value for Pt ($B_{\mathrm{Pt}} = 0.31$ Å^2).[30] During the fits, the total Mn occupancy integrated over all layers tends to diverge toward overestimated values, while increasing the Debye parameters, without any significant improvement on the fit quality. This total Mn occupancy is then fixed to the nominal value of 0.35 ML ($\theta^{\mathrm{tot}}_{\mathrm{Mn}} = 0.35$). The model giving the best fit involves only three atomic layers.

Figure 3(a) shows the experimental structure factors $|F_{HKL}|$ for the 0.35-ML Mn film together with the best fit for the (1 1)-CTR. Other two nonequivalent CTRs, (1 0) and (2 0), are also measured (not shown). Each of these three CTRs is averaged over two or three equivalent ones. The agreement between model and experiment is excellent. The structural parameters are summarized in Table I and a pictorial view is given in Fig. 4. The interlayer distances show limited variations. The distances d_0 and d_1 are respectively expanded and contracted as compared to the bulk, d_b. The value of the d_2 distance has a limited meaning, due to the low coverage of the last layer ($\theta^2_{\mathrm{Mn}} = 0.00$, $\theta^2_{\mathrm{Pt}} = 0.07$). The layer 0 does not contain any Mn atom, indicating a negligible interdiffusion. The Pt occupancy lower than 1 ($\theta^0_{\mathrm{Pt}} = 0.92$) indicates that this layer is not completely filled by cubic Pt(001)-(1×1). The remaining surface (8%) must be covered by the Pt(001)-hex reconstruction and does not contribute to the diffracted intensity in integer CTRs. This amount of reconstruction is in perfect agreement with that deduced from the rocking scan integration over the Pt(001)-hex peaks (see Fig. 2). Mn atoms are found only in layer 1. The total Pt occupancy of layers 1 and 2, $\theta^{1,2}_{\mathrm{Pt}} = 0.4$, means that an equivalent of 0.4-ML Pt is distributed into these two layers. This value is higher than the excess Pt atoms released by the deconstruction of layer (0.2 to 0.25 ML) and suggest that some additional Pt atoms have migrated likely from steps and domain borders to the surface. The B parameters associated to the layers ($B \approx 1.6$ Å^2) are much larger than those of bulk metals ($B_{\mathrm{Mn}} = 0.44$ Å^2 and $B_{\mathrm{Pt}} = 0.31$ Å^2),[30] denoting a large structural disorder.

This 0.35-ML Mn film was annealed to 520 K for 30 min and cooled down to RT. Only a residual part (3%) of the original reconstruction is preserved [see Fig. 2(d)]. The study of a complete data set collected along integer $(H\ K)$-CTRs [see Fig. 3(b) that shows the (1 1)-CTR] provides similar results, with a slightly better agreement factor ($\chi^2 = 1.5$). The Pt occupancy in layer 2 ($\theta^2_{\mathrm{Pt}} = 0.11$) is larger while the total amount of Pt in the surface remains the same ($\theta^{1,2}_{\mathrm{Pt}} = 0.4$), indicating that some additional Pt atoms have migrated to the overlayer during annealing. The important outcome here is that Mn atoms are also found only in layer 1. This demonstrates that Mn diffusion remains negligible even up to 520 K. The Debye parameters are reduced close to the bulk values ($B \approx 0.44$ Å^2), denoting a limited structural disorder.

B. 1.2-ML Mn deposited at RT, then covered by Pt

The deposition of 1.2-ML Mn at RT on a freshly cleaned substrate generates a surface structure in logical sequence to that observed in the case of the 0.35 ML deposition. The peaks of the Pt(001)-hex reconstruction are still present with

TABLE I. Structural parameters for the 0.35-ML and 1.2-ML Mn films deposited on the Pt(001)-hex surface at RT. θ(Pt/Mn), $d_\perp$ and B are the Pt/Mn atomic occupancies, the interlayer distances perpendicular to the surface and the Debye parameter, respectively.

sample	0.35-ML Mn			1.2-ML Mn		
layers	θ(Pt/Mn)	$d_\perp$[Å]	B[Å^2]	θ(Pt/Mn)	$d_\perp$	B
2	0.07(1)/0.00	2.12(3)	1.6(4)	0.00(2)/0.60(2)	∼2.08(2)	0.44
1	0.33(4)/0.35	1.956(4)	1.6(4)	0.39(2)/0.58(5)	1.951(2)	0.44
0	0.92(2)/0.00	1.976(2)	0.5(1)	0.97(1)/0.03(3)	1.999(1)	0.31
Bulk	1/0	1.962	0.31	1/0	1.962	0.31
χ^2		2.1			4.4	

a reduced intensity [see Fig. 2(e)] and similar traces of MnPt-$c(2\times2)$ surface alloy peaks are observed. The experimental curve and best fit are given in Fig. 3(c) for the (1 1)-CTR. The structural parameters resulting from the quantitative model of the CTRs are reported in Table I. The layer 0 is completely filled and contains only traces of Mn (≈3%). The layer 1 contains nonstoichiometric Mn and Pt mixture ($\theta^1_{\rm Mn}=0.58$ and $\theta^1_{\rm Pt}=0.39$). The layer 2 is essentially filled with the remaining Mn atoms ($\theta^2_{\rm Mn}=0.60$) with negligible amount of Pt atoms. There is no third surface layer, indicating that Mn on Pt(001) grows epitaxially in a layer-by-layer mode at RT. When Mn deposition is pursued up to 6 MLs clear intensity oscillations at the anti-phase (1 1 1) reciprocal space point can be observed (not shown), confirming this outcome.

Still at RT, 1 ML of Pt was deposited on the Mn(1.2ML)/Pt(001) surface. The CTRs intensity for a sandwich Pt/Mn/Pt(001) should increase at the antiphase positions. However, it is considerably reduced due to a largely increased roughness [see Fig. 3(d)]. Moreover, the Pt(001)-hex reconstruction is washed out [see Fig. 2(f)] and $c(2\times2)$ peaks are no longer detected. The structural model for the surface is similar to the previous one for the two first layers, with the addition of Pt islands on top of layer 2 using a β-like model.[21] In such model, each island layer (with label $m=0,1,2,\ldots$) has an occupancy given by $\theta_m=\theta_0\beta^m$. The fit indicates a limited Pt coverage ($\theta_0=0.17$) and a quite rough surface ($\beta=0.8$), which characterizes a 3D growth mode. The β parameter is related to the root-mean-square deviation by $\sigma_{\rm rms}=\beta^{1/2}/(1-\beta)\times d_\perp$, where $d_\perp$ is the distance between lattice planes perpendicular to the surface.[21] The model structure and interlayer distances are given in Fig. 4(b). The surface roughness, over the area defined by the x-ray coherent length (∼1000 nm), is $\sigma_{\rm rms}\approx 8.7$ Å.

C. Pt deposition at RT and at 600 K

Pt deposition on a clean Pt(001) surface was studied up to a few MLs. For Pt deposited at RT, growth intensity oscillations in the antiphase position are barely observable (open circles in Fig. 5). This points to a 3D growth mode and a rough surface, similar to that observed for the growth on the Mn(1.2 ML)/Pt(001) surface at RT.

At higher temperatures, we studied the deconstruction process by following the Pt(001)-hex peaks. We determined that a deposition at 600 K of 0.65-ML Pt reduces the reconstructed surface to nearly 20%, and of 0.8-ML Pt to less than 10%. After this initial deconstruction process, when Pt is further deposited at 600 K, clearly defined growth oscillations show up (full circles Fig. 5). Similar to Mn at RT, homoepitaxial growth of Pt at 600 K on a clean Pt(001) surface proceeds in a quasi layer-by-layer growth mode. The observation of a slightly decreasing intensity, superimposed to the growth oscillations, indicates that the growth slightly deviates from a perfect layer-by-layer mode owing to an increasing roughness. Nevertheless, the nearly completion of the Pt layer at such temperatures is sufficient to ensure the chemically ordered alternation of Mn and Pt planes perpendicular to the surface, as seen in the next section.

IV. MnPt THIN-FILM GROWTH

A. Alternate deposition at RT

Alternate depositions at RT of 1-ML Mn and 1-ML Pt, defined as 1-BL MnPt (BL for bilayer), were repeated six times to produce a MnPt film with a nominal thickness of ≈2.4 nm. The first 1-ML Mn was deposited directly on the Pt(001)-hex surface. The film was terminated by a 1-ML Pt deposition. Immediately after the 6-BL deposition, L scans were measured along the (1 1)-CTR and along the (1.03 1.03) position. The slightly shifted L scan gives the incoherent x-ray scattered background nearby the CTR (see Fig. 6). From the period of Kiessig oscillations (see Fig. 6), the film thickness was calculated to be ≈2.9 nm. This value is slightly higher than the nominal thickness of 2.4 nm and likely stems from variations in the source flux over the ∼5 hours deposition period.

For the RT grown film, labeled MnPt$_{\rm RT}$, the (1 1)-CTR intensity at the antiphase position ($L\approx1$) is washed out and

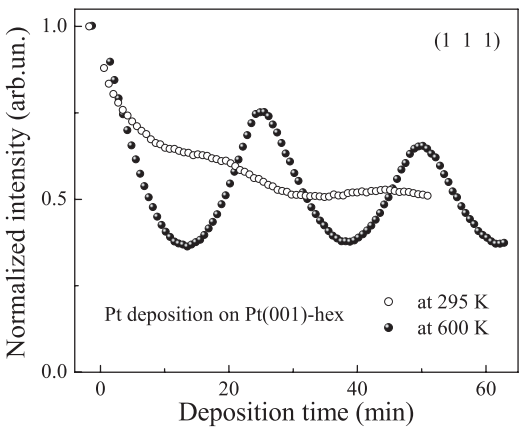

FIG. 5. Oscillations of the x-ray scattering intensity at the antiphase (1 1 1) reciprocal space point for Pt deposition on Pt(001)-hex at 295 K (open circles) and at 600 K (full circles).

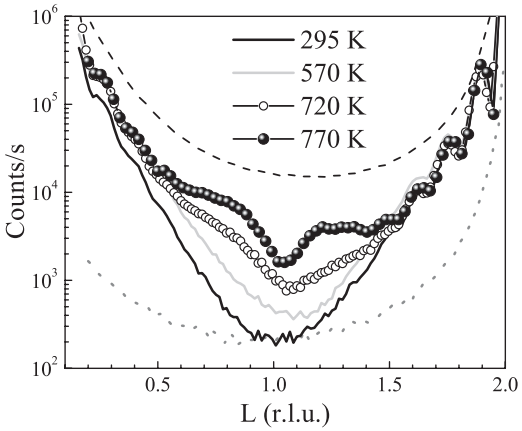

FIG. 6. L scans along the (1 1)-CTR at different annealing temperatures of the MnPt film grown at RT. Scans for the clean Pt(001)-hex surface (black dashed line) and background before annealing (gray dot line) are also shown.

reaches the background level (see Fig. 6). This indicates that the final surface is quite rough ($\sigma_{\rm rms} \approx 9$ Å), as expected from the results in the previous section. Around the (1 1 1) point, there is no trace of the order peak that would suggest the presence of the $L1_0$ MnPt phase with OP c axis. Likewise, no trace of $L1_0$ order peaks with in-plane (IP) c-axis orientationis found along the half-integer (1/2 1/2) rod.

The $\mathrm{MnPt_{RT}}$ film was then annealed from 295 up to 770 K by successive steps at increasing temperatures. Its structural evolution was monitored by measuring L scans along the (1 1)-CTR (see Fig. 6) and by checking the IP $L1_0$ order peak with rocking scans around the (1/2 1/2 0.15) reciprocal space point. Up to 570 K, no significant modification was detected. Above this temperature the intensity close to (1 1 1) starts to slightly increase in the L scans, while wide peaks appear in the (1/2 1/2 0.15) rocking scans. The evolution is stronger above 720 K, with an overall increase of the CTR intensity. The sample was finally kept at 770 K for 30 min. The scattered intensity in the antiphase region ($L \approx 1$) is recovered. The roughness has decreased one order of magnitude to $\sigma_{\rm rms} \approx$ 0.9 Å. The Kiessig oscillations are preserved, indicating that the layer has the same thickness (≈2.9 nm) as before annealing. This dismisses the possibility of Mn atoms diffusion into the substrate.

The heater was then turned off for the post-annealing structural study at RT. For this study a full set of L scans along nine (H K)-CTRs (among which six are nonequivalents) and rocking scans at selected (H K L) reciprocal space points were measured. Still, no peak related to the OP $L1_0$ phase is observed in the L scans along the crest of the CTRs. However, shifted L scans along the (1.03 1.03) show a broad peak around $L \approx 1.030$ [see Fig. 7(a)]. This peak corresponds to OP $L1_0$ short-range order (SRO) phase domains with limited correlation length. The L position and FWHM of such peaks, obtained by averaging over all (H K)-shifted L scans, provide, respectively, the average tetragonal distortion $[(c/a)^{\rm OP} = 1/L]$ and the correlation length $[\lambda_\perp^{\rm OP} \approx (1/\mathrm{FWHM})\, a_{\rm Pt}]$ of $L1_0$ MnPt domains with c axis perpendicular to the surface. The tetragonal distortion $(c/a)^{\rm OP} = 0.971 \pm 0.004$ is found to be larger than the bulk $L1_0$ MnPt one $[(c/a)^{\rm bulk} = 0.916]$ but in

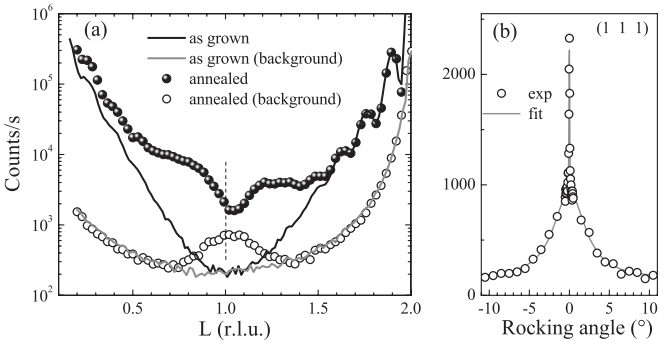

FIG. 7. (a) L scans along the (1 1)-CTR for the $(\mathrm{MnPt})_6$ film as deposited at RT (black solid line) and after annealing at 770 K (full circles). The offset scans, along (1.03 1.03), before annealing (gray solid line) give the background, and after annealing, show a broad peak coming from $L1_0$ domains. The vertical (dash) line indicates the position for the rocking scan shown in (b).

remarkable agreement with the value expected for pseudomorphic growth with a constant unit cell volume (≈0.97). The Poisson ratio is 0.493, very close to the value 0.5 expected for a perfectly elastic deformation at constant volume. We deduce that the film is pseudomorphically strained and, moreover, that it possess a stoichiometry close to the expected (1:1) value. The correlation length $\lambda_\perp^{\rm OP} \approx 1.7 \pm 0.3$ nm is lower than the film thickness (≈2.9 nm), indicating that the film is not ordered over its whole thickness. An extended rocking scan at the (1 1 1) reciprocal space point reveals that a broad peak is superimposed to the sharp CTR peak [see Fig. 7(b)]. This broad peak, associated to the OP $L1_0$ SRO domains, provides an estimation of their correlation length parallel to the surface, $\lambda_\parallel^{\rm OP} \approx (1/\mathrm{FWHM})\,(a_{\rm Pt}/\sqrt{2}) = 2.5 \pm 0.2$ nm.

The diffracted intensity along the half-integer rods, (1/2 1/2) or (3/2 3/2), originates from $L1_0$ domains with IP c-axis orientation. The Lscan for the (1/2 1/2) rod [see Fig. 8] shows broad peaks at $L \approx 1$ and $L \approx 2$ corresponding, respectively, to IP $L1_0$ domains with c axis oriented along the [1 1 0] and [1 $\bar{1}$ 0] directions, indexed in the surface cell. These directions are totally equivalent, so that the IP-$L1_0$ MnPt domains form a twinned structure parallel to the surface. From the average position and width of those peaks, we determined the tetragonal distortion and the correlation length perpendicular to the surface: $(b/a)^{\rm IP} = 1/L = 0.968 \pm 0.006$ and $\lambda_\perp^{\rm IP} \approx$

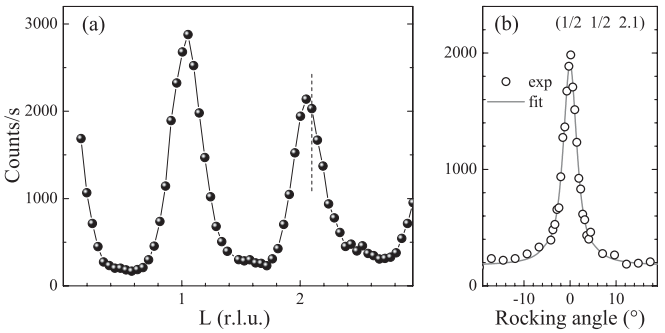

FIG. 8. (a) L scan along the (1/2 1/2)-rod for the MnPt film deposited at RT and annealed at 770 K. The vertical (dash) line indicates the position for the rocking scan shown in (b).

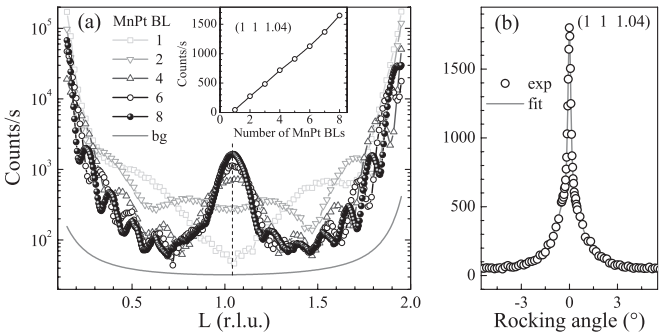

FIG. 9. (a) L scans along the (1 1)-CTR during MnPt deposition at 570 K for 1, 2, 4, 6, and 8 (closed circle) MnPt BLs; the background is also shown (gray solid line). Inset: counts at the (1 1 1.04) reciprocal space point (indicated by vertical dashed line) as a function of the number of deposited MnPt BLs. (b) Rocking scan around the (1 1 1.04) reciprocal space point for the 8-BL film.

(1/FWHM) $(a_{\mathrm{Pt}}/\sqrt{2}) = 1.4 \pm 0.2$ nm, respectively. Since the $L1_0$ c axis is parallel to the surface, the tetragonal distortion of the IP domains, imposed by the pseudomorphic epitaxy, is along the b axis defined for the MnPt structure. The volume of the unit cell, calculated considering a pseudomorphic strain, agrees with the bulk MnPt one within 0.3%. From a rocking curve at (1/2 1/2 2.1) [see Fig. 8(b)], we deduce the correlation length parallel to the surface of $\lambda_{\parallel}^{\mathrm{IP}} \approx 6.3 \pm 0.7$ nm.

B. Alternate deposition at 570 K

A new film was grown with the substrate held at 570 K during the whole deposition. As a preliminary step, 1 ML of Pt was deposited on the clean Pt(001)-hex surface, so that almost all surface was deconstructed back to the Pt(001)-(1 × 1). According to the results of Sec. III, this procedure aims to minimize the interface alloying among Mn and Pt in the earliest growth stage. Alternate depositions of 1-ML Mn and 1-ML Pt were then repeated 8 times to produce a film, labeled $\mathrm{MnPt_{HT}}$, with nominal thickness of ≈3.0 nm, terminated by a Pt layer. After each MnPt BL deposition, a fast L scan along the (1 1)-CTR and a rocking scan at the (1/2 1/2 0.15) reciprocal space point were collected.

Figure 9 shows the CTRs at successive stages of the film growth. After the first BL, the CTR shows a dip in the antiphase region ($L \approx 1$) and two side minima for $L \approx 0.3$ and $L \approx 1.7$. This general shape suggests an alloying process. This is confirmed by rocking scans at (1/2 1/2 0.15) showing traces of a MnPt-$c(2 \times 2)$ peak. With 2-BL deposition, the antiphase intensity increases, but a local minimum and side minima are is still present. Above 3 BL, an OP $L1_0$ order peak clearly shows up around $L \approx 1.04$. This remarkably differentiates the third MnPt BL from the two precedents. At a variance with the case of the RT deposition, the OP $L1_0$ order peak is here visible in the CTR itself, indicating a much better chemically ordered structure. The order peak becomes sharper and more intense with the number of BLs. The evolution of its intensity is given in the inset of Fig. 9(a). The linear increase of this intensity demonstrates that the pseudomorphic growth and chemical order are maintained up to 8 MnPt BLs.

The heater was turned off and a thorough structural study was performed. A full set of L scans along eight (H K)-CTRs (among which five nonequivalents) and rocking scans at selected (H K L) reciprocal space points were collected. The OP $L1_0$ peak positions and widths were averaged over all CTRs, providing the characteristic values for the OP $L1_0$ domains : $(c/a)^{\mathrm{OP}} = 0.960 \pm 0.001$ and $\lambda_{\perp}^{\mathrm{OP}} \approx 2.9 \pm 0.1$ nm. The correlation length parallel to the surface is $\lambda_{\parallel}^{\mathrm{OP}} \approx 6.6 \pm 0.6$ nm, obtained from the rocking scan at the (1 1 1.04) reciprocal space point [see Fig. 9(b)]. A radial scan at this position yields an H (and K) value of 0.997 ± 0.005, showing that these domains are pseudomorphic within an accuracy of 0.5%.

Twinned $L1_0$ domains with IP c-axis orientation are also observed for this film through L scans performed along half-integer rods. The analysis of peak position and FWHM yields a tetragonal distortion and a perpendicular correlation length of $(b/a)^{\mathrm{IP}} = 0.979 \pm 0.003$ and $\lambda_{\perp}^{\mathrm{IP}} \approx 2.7 \pm 0.2$ nm, respectively. The rocking scan analysis gives a parallel correlation length of $\lambda_{\parallel}^{\mathrm{IP}} \approx 4.1 \pm 0.3$ nm and a radial scan at the (1/2 1/2 1.02) reciprocal space point shows that these $L1_0$ IP domains are also pseudomorphic within an accuracy of 0.5%.

Another film was deposited at an intermediate temperature, 500 K. The roughness is significantly decreased compared to the RT grown film, but no chemical order peaks are observed, only a faint intensity in a large rocking scan at the antiphase (1 1 1) position. Even with post-growth annealing at 670 K for 7 hours the OP $L1_0$ domains are only slightly increased and remain comparable to the RT deposition.

To summarize this section, we have described the growth by alternate deposition and the structure of two MnPt ultrathin (≈3.0 nm) films: $\mathrm{MnPt_{RT}}$, grown at RT then annealed to 770 K, and $\mathrm{MnPt_{HT}}$, grown at 570 K. The $\mathrm{MnPt_{RT}}$ film exhibits IP-$L1_0$ domains, with variants along the [110] and [1$\bar{1}$0] directions that are more than twice larger compared to the OP ones. The $\mathrm{MnPt_{HT}}$ film, on the other hand, exhibits OP-$L1_0$ domains ([001] variant) larger than the IP variants. Quantitative results are reported in Table. II, along with the correlation volume of the chemically ordered domains, calculated as $V_{\lambda} = \lambda_{\parallel} \times \lambda_{\parallel} \times \lambda_{\perp}$. We note that the domain sizes are comparable to those found in polycrystalline sputtered films used in EB applications.[31] Moreover, we should point out that the crystallographic order of both $\mathrm{MnPt_{RT}}$ and $\mathrm{MnPt_{HT}}$ films presents a correlation length much larger than the size of these OP-$L1_0$ and IP-$L1_0$ SRO domains. The FWHM of the sharp component of the CTRs peak [e.g., Fig. 7(b)] yields a correlation length of ≈150–200 nm along both [110] and [1$\bar{1}$0] directions. Over such an area, which corresponds to the average terraces on the MnPt/Pt(001) surface, the crystallographic order is perfect, apart from some thermal and structural disorder represented by the Debye parameter. The different variants are only related to the nucleation of chemical order along orthogonal directions or to anti-phase domains. From the crystallographic point of view, the MnPt film is epitaxial and pseudomorph with no grain boundaries over the terraces. From the integrated intensities of the superlattice peaks compared to the full CTRs, we found that about (90 ± 10)% of the film is chemically ordered. A real space schematic representation of these structural results is given in Fig. 10.

TABLE II. Tetragonal distortion and morphological parameters for the films grown at RT and at 570 K. OP and IP stand for out-of-plane and in-plane, respectively.

	film $MnPt_{RT}$		film $MnPt_{HT}$	
	OP	IP	OP	IP
c/a (b/a)	0.971 ± 0.004	0.968 ± 0.006	0.960 ± 0.001	0.979 ± 0.003
$\lambda_\perp$ (nm)	1.7 ± 0.3	1.4 ± 0.2	2.9 ± 0.1	2.7 ± 0.2
$\lambda_\parallel$ (nm)	2.5 ± 0.2	6.3 ± 0.7	6.6 ± 0.6	4.1 ± 0.3
V_λ (nm^3)	~ 11	~ 56	~ 126	~ 45

V. EXCHANGE BIAS PROPERTIES OF FM/MnPt EXCHANGE-COUPLED LAYERS

In this section, we discuss the magnetic properties, studied by magnetooptic Kerr effect (MOKE), of the systems formed by coupling the $MnPt_{RT}$ and $MnPt_{HT}$ films to FM layers. We intentionally combine the first film with a FM layer with planar magnetic anisotropy and the second one with a FM layer showing perpendicular magnetic anisotropy. MOKE measurements were carried out in the ultrahigh vacuum multichamber system at Max-Plank-Institut für Mikrostrukturphysik in Halle, Germany.

A. Fe/$MnPt_{RT}$ / Pt(001)

In order to establish the characteristics of the Fe layer that will be grown on the MnPt layer to probe its AFM properties, at first we studied the growth of an Fe layer on a similar MnPt/Pt(001) film by *in situ* GIXRD. We observed that the Fe layer does not relax up to 18 ML. Up to this thickness, the layer is tetragonal bct pseudomorphically strained on the MnPt/Pt(001) film with $a_{Fe\parallel} = (a_{Pt}/\sqrt{2}) = 2.775$ Å and $a_{Fe\perp} = 3.042$ Å. This gives a tetragonal distortion of $(a_\perp/a_\parallel)_{Fe} = 1.28$ and a unit cell volume very close to the bcc bulk Fe.

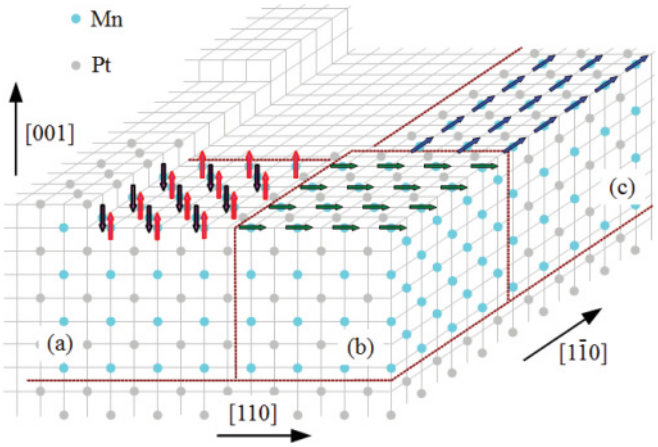

FIG. 10. (Color online) Schematic real-space representation of the MnPt/Pt(001) surface. A large terrace close to one border is represented, as well as three different chemically ordered $L1_0$ domains: one domain with the c axis perpendicular to the surface (a), one with the c axis along the [110] direction (b), and one along the [1$\bar{1}$0] direction (c). For the [001] domain, the Mn spins surface is completely compensated, while for the other two, the Mn spins give rise to uncompensated surface layers. Crystallographic axes are indicated in the surface lattice. Only surface spins are shown.

The $MnPt_{RT}$ film was covered *in situ* at RT with 15-ML Fe layer and protected against oxidation by 10-ML Pt. The film grows with bct Fe[001] axis perpendicular to the (001)-plane surface and with the Fe[100] axis parallel to the fcc Pt [110] and MnPt[110] axes. In these conditions, the FM Fe easy axes, [100] and [010], are 45° away from the spin axes of the twinned IP-$L1_0$ MnPt domains. *Ex situ* x-ray specular reflectivity confirms the nominal thicknesses of the different layers of the Pt(1.8 nm)/Fe(2.4 nm)/$MnPt_{RT}$(2.9 nm)/Pt(001) film and attests of a rather small roughness in the Fe/MnPt interface (≈0.9 Å).

Ex situ MOKE measurements in longitudinal geometry were carried out at RT, then at 5 K after magnetic field cooling ($H_{MFC} = 3000$ Oe) applied parallel to the Fe easy axis ($H_{MFC} \parallel$ Fe[001]). Hysteresis loops were measured along the same axis [see Fig. 11(a)]. At RT, the loop is narrow with a coercivity $H_C \approx 65$ Oe. At 5 K, the loops are clearly shifted along the magnetic field axis and broader than at RT. This shows that the $L1_0$ MnPt domains are AFM and that a given amount of uncompensated Mn spins are exchange coupled with the Fe spins at the FM/AFM interface. For the first loop at 5 K, the coercivity is $H_C \approx 336$ Oe, five times larger than at RT, and the EB shift is $H_{EB} \approx -170$ Oe. When the hysteresis loops are repeated several times, H_C and H_{EB} monotonically decrease as a function of the number of loops measured [see Fig. 11(b)]. This decrease, known as training effect, is associated to rearrangements of the spin structure

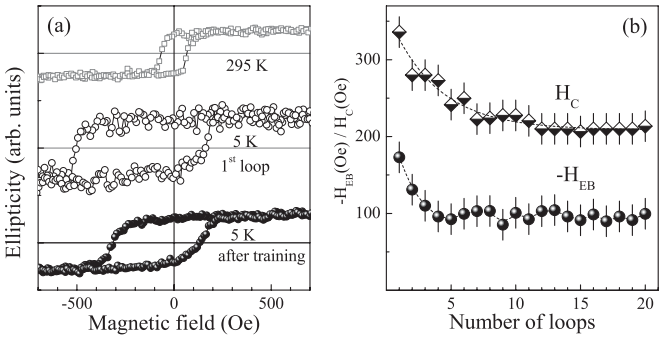

FIG. 11. (a) Longitudinal MOKE hysteresis loops of the Pt/Fe/$MnPt_{RT}$ film along the [100] Fe easy axis at 295 K (squares) and after magnetic field cooling ($H_{MFC} = 3000$ Oe) to 5 K (open circles) first loop and (closed circles) average from loop 10 to 20. (b) Coercivity (H_C) and exchange bias shift ($-H_{EB}$) as a function of the number of loops. (Lines are guides to the eye.)

towards equilibrium, because the spin configuration created after the field cooling is not thermodynamically stable.[32,33] Only the stable IP-$L1_0$ domains, with uncompensated spins along the [110] and [1$\bar{1}$0] directions (see Fig. 10), contribute to the stable EB shift.

B. FePt/MnPt$_{HT}$ / Pt(001)

The MnPt$_{HT}$ film was covered *in situ* by an FePt layer grown by alternate deposition of 1-ML Fe and 1-ML Pt at 570 K repeated four times. Then, it was protected by 8-ML Pt, giving a Pt(1.6 nm)/FePt(1.6 nm)/MnPt$_{HT}$(3.0 nm)/Pt(001) film. The lattice mismatch between FePt and Pt (and the pseudomorphic MnPt layer) favors the OP-$L1_0$ FePt c-axis orientation. *In situ* GIXRD characterization confirms that the FePt thin layer is pseudomorphic, with $c_{FePt} = 3.595$ Å along the [001] direction. The unit cell volume corresponds to the bulk $L1_0$ FePt, but with an increased tetragonal distortion $(c/a)_{FePt} = 0.916 \pm 0.002$. This increased tetragonal distortion leads to an enhanced perpendicular magnetic anisotropy.[8] The FePt/MnPt interface roughness given by x-ray reflectivity is here ≈2.5 Å. This value is larger than for the film grown at RT and annealed (MnPt$_{RT}$), but still of the order of one atomic step.

Ex situ polar MOKE measurements were carried out at RT, then at 5 K after magnetic field cooling ($H_{MFC} = 3000$ Oe) applied perpendicular to the film surface, i.e., along the FePt easy axis [see Fig. 12(a)]. At RT, the loop is narrow with a coercivity $H_C \approx 78$ Oe. At 5 K, hysteresis loops show much larger coercivity ($H_C \approx 720-760$ Oe) than at RT and display a small EB shift ($H_{EB} \approx -80$ Oe) that vanishes after a few loops measured [see Fig. 12(b)]. The absence of out-of-plane EB is the expected stable situation, as far as the AFM MnPt spin structure (see Fig. 1) is concerned. The magnetic field cooling from RT down to 5 K creates a metastable state with uncompensated spins that are responsible for the initial EB shift. However, once the field is switched back and forth, thermal excitation leads the system to the thermodynamically stable state.[31,32] In a perfect MnPt/FePt interface, there is no net OP Mn spin component (see Fig. 10) to couple with the OP FM spins and to give rise to a unidirectional anisotropy.

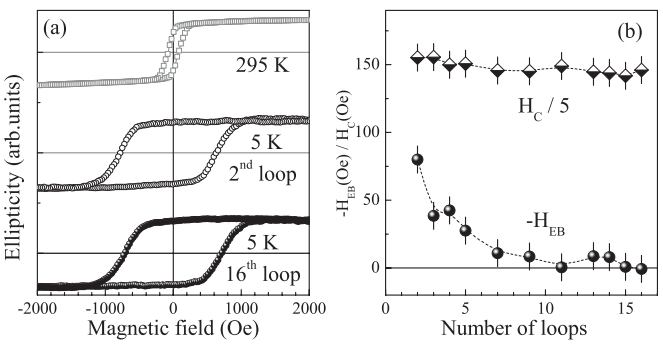

FIG. 12. (a) Polar MOKE hysteresis loops of the Pt/FePt/MnPt$_{HT}$ film at 295 K (squares) and after perpendicular magnetic field cooling ($H_{MFC} = 3000$ Oe) down to 5 K: (open circles) second loop and (closed circles) sixteenth loop. (b) Coercivity (H_C) and exchange bias shift ($-H_{EB}$) as a function of the number of loops measured. (Lines are guides to the eye.)

VI. DISCUSSION

We have performed a study of the growth process of chemically ordered $L1_0$ MnPt ultrathin films, starting from the earliest stages up to the completion of ≈3.0-nm thin films. We demonstrate that epitaxial growth of Mn on a clean Pt(001) surface is affected by the Pt(001)-hex reconstruction. When Mn is deposited, it lifts locally the reconstruction. The high mobility of atoms caused by this process leads to the formation of an ordered MnPt-$c(2 \times 2)$ surface alloy with the excess of Pt atoms from the deconstructed layer. The removal of the reconstruction prior to Mn deposition is an important issue in order to inhibit such alloying. This removal can be achieved by Pt homoepitaxial deposition. However, we observed that some alloying persists, whatever the thermal conditions of the deposition. The alloying may possibly still be reduced by H passivation,[34] but this has not been used in the present study. This surface alloying, however, does not preclude anisotropic $L1_0$ growth.

The choice of the temperature for Pt deposition on Pt(001) and on Mn/Pt(001) turns out to be much more critical than the initial alloying. At RT, Pt deposition proceeds mostly in a 3D mode, leading to quite a rough surface composed by islands. The formation of 3D Pt islands on the surface at RT is not surprising[35] and can be directly related to a reflection barrier for Pt atoms to jump down step edges.[36] As a consequence, subsequent Mn deposition leads to large intermixing and alloying. Alternate deposition of Mn and Pt at RT yields a rough and disordered MnPt film. Post-growth annealing (up to 770 K) smoothes the surface and gives rise to small $L1_0$ MnPt domains without any observable Mn diffusion into the bulk. All three possible variants with c axis along the [001], [110], and [1$\bar{1}$0] directions are observed. However, the OP-$L1_0$ MnPt domains are much smaller (≈2.5 nm) than the twinned IP ones (≈6.3 nm) (see Table II). If one considers the relative surface area, $\{(2.5 \times 2.5/[2(6.3 \times 6.3)] \approx 8\%\}$, such a film has essentially an IP biaxial magnetocrystalline anisotropy with uncompensated surface magnetization. A similar twinned domain structure was observed in thicker MnPt films (≈30 nm) grown by thermal co-deposition of Pt and Mn at RT. In these films transmission electron microscopy revealed the existence of chemically ordered 8-nm crystallites with the two orthogonal IP c-axis orientations.[37,38]

When our film grown at RT, MnPt$_{RT}$, is covered by an Fe layer with IP magnetocrystalline anisotropy, an increased coercivity and exchange bias shift at 5 K demonstrate that the Mn spins of the twinned domains are exchange-coupled with Fe spins at the FM/AFM interface. In addition, the gradual decrease of H_{EB} with the number of loops measured is a macroscopic indication that a rearrangement of the spin structure toward equilibrium is taking place. Upon repeated loops at 5 K, the exchange bias shift H_{EB} is stabilized at $H_{EB} \approx 100$ Oe, showing that a significant amount of uncompensated spins in frozen AFM domains is preserved. $H_C \approx 210$ Oe at 5 K is still about three times larger than at RT. The stable exchange bias shift corresponds to an additional interface energy of $\Delta\sigma = | H_{EB} | M_s t_{FM}$,[3,4] which gives $\Delta\sigma \approx 0.042 \text{erg/cm}^2$, using $M_s = 1752 \text{erg/cm}^3$, and $t_{FM} \approx 2.4$ nm. We can conclude that the AFM magnetocrystalline anisotropy in IP-$L1_0$ MnPt domains as small as a few nanometers is large

enough to induce a stable unidirectional anisotropy in the Fe layer.

The growth at higher temperatures yields a rather different $MnPt_{HT}$ film. Pt deposition at ≈570 K provides a quasi layer-by-layer growth. After Mn deposition, no significant Mn diffusion into the Pt bulk is observed. Consequently, alternate deposition of Mn and Pt at 570 K yields a much better chemically ordered film. The OP-$L1_0$ order peak is clearly distinguished in the antiphase region of the CTRs during the growth [see Fig. 9(a)]. The OP-$L1_0$ MnPt domains appear to be much larger but still coexist with twinned IP ones (see Table II). Both OP and IP domains have a perpendicular correlation length very close to the nominal film thickness (≈3.0 nm). However, in contrast to the case of $MnPt_{RT}$, the OP-$L1_0$ domains are larger than the IP ones. The volume of the OP-$L1_0$ domains is more than one order of magnitude larger for the present $MnPt_{HT}$ film compared to the $MnPt_{RT}$ one. This should have implications on the magnetic properties, in particular, on the AFM magnetocrystalline anisotropy energy that scales with the domain volume.

When the $MnPt_{HT}$ film is coupled to a FePt layer with PMA, a clear exchange bias shift is observed at 5 K. The exchange bias shift of the first loop corresponds to an additional interface energy of $\Delta\sigma \approx 0.015 \mathrm{erg/cm^2}$, using $M_s = 1140 \mathrm{erg/cm^3}$, and $t_{FM} \approx 1.6$ nm. After a few training loops, the system relaxes to an equilibrium state and the exchange bias vanishes. As far as the AFM spin structure is concerned, this is the expected thermodynamically stable configuration, since the interface of the OP-$L1_0$ MnPt domains is compensated and no net out-of-plane AFM magnetization is expected. Nevertheless, the coercivity remains large (nearly constant at $H_C \approx 720$ Oe) since the exchange coupling between Fe and Mn spins is always present.

In summary, the first stages of growth of Mn and Pt on clean Pt(001) substrate are studied quantitatively at different temperatures. Then, ≈3.0 nm-MnPt thin films are grown at different temperature conditions. The film grown at RT and annealed at 770 K presents chemically ordered $L1_0$ domains essentially with in-plane anisotropy. When coupled with a FM Fe layer, with in-plane anisotropy as well, stable exchange bias shift and larger coercivity are observed, indicating a net magnetization in the interface of the AFM domains. Optimized growth conditions at 570 K provide a chemically-ordered MnPt thin film with out-of-plane tetragonal ($L1_0$) c axis. Coupled to a FM FePt layer showing perpendicular magnetic anisotropy, such thin film shows promising out-of-plane exchange coupling properties.

ACKNOWLEDGMENTS

We acknowledge beam time at the French CRG BM32 beamline at the European Synchrotron Radiation Facility (ESRF). M.M.S. acknowledges the scholarship from the Fondation Nanoscience, Grenoble, France.

*Present address: Department of Physics, Universidade Federal de Pernambuco, 50670-901 Recife, Brazil.
†helio.tolentino@grenoble.cnrs.fr
‡Present address: Department of Physics, Gebze Institute of Technology, 41400 Kocaeli, Turkey.

[1] W. H. Meiklejohn and C. P. Bean, Phys. Rev. **105**, 904 (1957).
[2] A. P. Malozemoff, Phys. Rev. B **35**, 3679 (1987).
[3] J. Nogues and I. K. Schuller, J. Magn. Magn. Mater. **192**, 203 (1999).
[4] M. Kiwi, J. Magn. Magn. Mater. **234**, 584 (2001).
[5] E. Krén, G. Kádár, L. Pál, J. Sólyom, P. Szabó, and T. Tarnóczi, Phys. Rev. **171**, 574 (1968).
[6] J. P. Nozieres, S. Jaren, Y. B. Zhang, A. Zeltser, K. Pentek, and V. S. Speriosu, J. Appl. Phys. **87**, 3920 (2000).
[7] A. Cebollada, D. Weller, J. Sticht, G. R. Harp, R. F. C. Farrow, R. F. Marks, R. Savoy, and J. C. Scott, Phys. Rev. B **50**, 3419 (1994).
[8] M. M. Soares, H. C. N. Tolentino, M. D. Santis, A. Y. Ramos, and J. C. Cezar, J. Appl. Phys. **109**, 07D725 (2011).
[9] F. Yildiz, F. Luo, C. Tieg, R. M. Abrudan, X. L. Fu, A. Winkelmann, M. Przybylski, and J. Kirschner, Phys. Rev. Lett. **100**, 037205 (2008).
[10] M. F. Toney, M. G. Samant, T. Lin, and D. Mauri, Appl. Phys. Lett. **81**, 4565 (2002).
[11] T. Sato, M. Tsunoda, and M. Takahashi, J. Magn. Magn. Mater. **240**, 277 (2002).
[12] Y. S. Choi, A. K. Petford-Long, R. C. C. Ward, R. Fan, J. P. Goff, and T. P. A. Hase, J. Appl. Phys. **99**, 083903 (2006).
[13] P. Villars and L. D. Calvert, *Pearson's Handbook of Crystallographic Data for Intermetallic Phases* (American Society for Metals, Metals Park, OH, 1985).
[14] Z. Lu, R. V. Chepulskii, and W. H. Butler, Phys. Rev. B **81**, 094437 (2010).
[15] D. L. Abernathy, S. G. J. Mochrie, D. M. Zehner, G. Grübel, and D. Gibbs, Phys. Rev. B **45**, 9272 (1992).
[16] A. Borg, A.-M. Hilmen, and E. Bergene, Surf. Sci. **306**, 10 (1994).
[17] S. M. Valvidares, T. Schroeder, O. Robach, C. Quirós, T.-L. Lee, and S. Ferrer, Phys. Rev. B **70**, 224413 (2004).
[18] K. He, L. J. Zhang, X. C. Ma, J. F. Jia, Q. K. Xue, and Z. Q. Qiu, Phys. Rev. B **72**, 155432 (2005).
[19] W. Kim, S. C. Hong, J. Seo, S.-J. Oh, H. G. Min, and J.-S. Kim, Phys. Rev. B **70**, 174453 (2004).
[20] R. Baudoing-Savois *et al.*, Nucl. Instrum. Methods Phys. Res., Sect. **149**, 213 (1999).
[21] I. K. Robinson, Phys. Rev. B **33**, 3830 (1986).
[22] E. Weschke, C. Schüßler-Langeheine, R. Meier, G. Kaindl, C. Sutter, D. Abernathy, and G. Grübel, Phys. Rev. Lett. **79**, 3954 (1997).
[23] E. Vlieg, J. Appl. Crystallogr. **30**, 532 (1997).
[24] X. Torrelles and J. Rius, J. Appl. Crystallogr. **37**, 395 (2004).
[25] I. K. Robinson, *Handbook of Synchrotron Radiation* (North Holland, Amsterdam, 1991), Vol. 3.
[26] E. Vlieg, J. Appl. Crystallogr. **33**, 401 (2000).
[27] B. Warren, *X-ray Diffraction* (Addison-Wesley, Boston, MA, USA, 1969).
[28] M. M. Soares, Ph.D. thesis, Université Joseph Fourier, 2011.

[29]M. De Santis, Y. Gauthier, H. C. N. Tolentino, G. Bihlmayer, S. Blügel, and V. Langlais, Phys. Rev. B **75**, 205432 (2007).
[30]C. H. Macqillavry, G. D. Rieck, and K. Lonsdale, *International Tables for X-ray Crystallography*, 2nd ed. (Kynoch Press, Birmingham, 1968), Vol. III.
[31]K. O'Grady, L. Fernandez-Outon, and G. Vallejo-Fernandez, J. Magn. Magn. Mater. **322**, 883 (2010).
[32]C. Binek, Phys. Rev. B **70**, 014421 (2004).
[33]F. Radu and H. Zabel, in *Magnetic Heterostructures*, edited by H. Zabel and S. Bader, Springer Tracts in Modern Physics Vol. 227 (Springer, Berlin/Heidelberg, 2008), pp. 97–184.
[34]M. Wakisaka, M. Sugimasa, J. Inukai, and K. Itaya, J. Electrochem. Soc. **150**, E81 (2003).
[35]T. R. Linderoth, J. J. Mortensen, K. W. Jacobsen, E. Lægsgaard, I. Stensgaard, and F. Besenbacher, Phys. Rev. Lett. **77**, 87 (1996).
[36]G. Kellogg, Surf. Sci. **246**, 31 (1991).
[37]A. Mougin, J. Borme, R. L. Stamps, A. Marty, P. Bayle-Guillemaud, Y. Samson, and J. Ferré, Phys. Rev. B **73**, 024401 (2006).
[38]J. Borme, Ph.D. thesis, Université Joseph Fourier, 2006.